arXiv:astro-ph/0503085v1 3 Mar 2005

Spectrum of Very High Energy Gamma-Rays from the blazar 1ES 1959+650 during flaring activity in 2002.

M. K. Daniel[1], H. M. Badran[2], I. H. Bond[3], P. J. Boyle[4], S. M. Bradbury[3], J. H. Buckley[5], D. A. Carter-Lewis[1], M. Catanese[6], O. Celik[7], P. Cogan[10], W. Cui[8], M. D'Vali[3], I. de la Calle Perez[3], C. Duke[9], A. Falcone[8], D. J. Fegan[10], S. J. Fegan[6,19], J. P. Finley[8], L. F. Fortson[4], J. A. Gaidos[8], S. Gammell[10], K. Gibbs[6], G. H. Gillanders[11], J. Grube[3], J. Hall[12], T. A. Hall[13], D. Hanna[14], A. M. Hillas[3], J. Holder[3], D. Horan[6], T. B. Humensky[4], A. Jarvis[7], M. Jordan[5], G. E. Kenny[11], M. Kertzman[15], D. Kieda[12], J. Kildea[15], J. Knapp[3], K. Kosack[5], H. Krawczynski[5], F. Krennrich[1], M. J. Lang[11], S. Le Bohec[1,12], E. Linton[4], J. Lloyd-Evans[3], A. Milovanovic[3], P. Moriarty[16], D. Müller[4], T. Nagai[12], S. Nolan[8], R. A. Ong[7], R. Pallassini[3], D. Petry[17], B. Power-Mooney[10], J. Quinn[10], M. Quinn[16], K. Ragan[14], P. Rebillot[5], P. T. Reynolds[18], H. J. Rose[3], M. Schroedter[6,19], G. H. Sembroski[8], S. P. Swordy[4], A. Syson[3], V. V. Vassiliev[12], S. P. Wakely[4], G. Walker[12], T. C. Weekes[6] and J. Zweerink[7]

mkdaniel@iastate.edu

ABSTRACT

The blazar 1ES 1959+650 was observed in a flaring state with the Whipple 10 m Imaging Atmospheric Cherenkov Telescope during May of 2002. A spectral analysis has been carried out on the data from that time period and the resulting very high energy gamma-ray spectrum ($E \geq 316\,\mathrm{GeV}$) can be well fit by a power-law of differential spectral index $\alpha = 2.78 \pm 0.12_{\mathrm{stat.}} \pm 0.21_{\mathrm{sys.}}$. On June 4th 2002, the source flared dramatically in the gamma-ray range without any coincident increase in the X-ray emission, providing the first unambiguous example of an 'orphan' gamma-ray flare from a blazar. The gamma-ray spectrum for these data can also be described by a simple power-law fit with $\alpha = 2.82 \pm 0.15_{\mathrm{stat.}} \pm 0.30_{\mathrm{sys.}}$. There is no compelling evidence for spectral variability, or for any cut-off to the

[1]Department of Physics and Astronomy, Iowa State University, Ames, IA 50011-3160, USA

[2]Physics Department, Tanta University, Tanta, Egypt

[3]Department of Physics, University of Leeds, Leeds, LS2 9JT, Yorkshire, England, UK

[4]Enrico Fermi Institute, University of Chicago, Chicago, IL 60637, USA

[5]Department of Physics, Washington University, St. Louis, MO 63130, USA

[6]Fred Lawrence Whipple Observatory, Harvard-Smithsonian CfA, P.O. Box 97, Amado, AZ 85645-0097, USA

[7]Department of Physics, University of California, Los Angeles, CA 90095-1562, USA

[8]Department of Physics, Purdue University, West Lafayette, IN 47907, USA

[9]Department of Physics, Grinnell College, Grinnell, IA 50112-1690, USA

[10]Experimental Physics Department, National University of Ireland, Belfield, Dublin 4, Ireland

[11]Department of Physics, National University of Ireland, Galway, Ireland

[12]High Energy Astrophysics Institute, University of Utah, Salt Lake City, UT 84112, USA

[13]Department of Physics and Astronomy, University of Arkansas at Little Rock, Little Rock, AR 72204-1099, USA

[14]Physics Department, McGill University, Montreál, QC H3A 2T8, Canada

[15]Department of Physics and Astronomy, DePauw University, Greencastle, IN 46135-0037, USA

[16]School of Science, Galway-Mayo Institute of Technology, Galway, Ireland

[17]University of Maryland, Baltimore County and NASA/GSFC, USA

[18]Department of Applied Physics and Instrumentation, Cork Institute of Technology, Cork, Ireland

[19]Department of Physics, University of Arizona, Tucson, AZ 85721

spectrum.

Subject headings: BL Lacertae objects: individual (1ES1959+650) — gamma-rays: observations — techniques: spectroscopic

1. Introduction

The electromagnetic emission from the blazar sub-classification of active galactic nuclei (AGN) is dominated by a highly variable non-thermal component. The emission extends from the radio to the gamma-ray and is believed to be produced in a highly relativistic plasma jet aligned closely to the line of sight. In a νF_ν representation the spectral energy distribution (SED) displays two broad peaks: the lower energy peak is generally attributed to synchrotron radiation from a population of relativistic electrons; the higher energy peak is mostly thought to be due to inverse Compton scattering from that electron population. The seed photon field for the Compton upscattering could have many origins: in the synchrotron self-Compton (SSC) models it is the synchrotron photons from the relativistic electrons themselves (Maraschi, Ghisellini & Celotti 1992); in external Compton models it could be due to photons emitted by an accretion disc (Dermer, Schlickeiser & Mastichiadis 1992), or reflected from emission line clouds (Sikora, Begelman & Rees 1994). Alternative theories for the origin of the high energy emission involve a hadronic precursor, such as the decay of pions formed in cascades generated by a high energy proton beam crossing a target in the jet (Atoyan et al. 2002), or from proton synchrotron radiation (Mücke et al. 2003).

Observations taken with the Whipple 10 m telescope in May-July of 2002 caught 1ES 1959 in a flaring state (Holder et al. 2003), with a mean flux of 0.64 ± 0.03 times the steady Crab Nebula flux and reaching 5 times that of the Crab at maximum. These observations were quickly followed up and confirmed by the HEGRA (Aharonian et al. 2003) and CAT (Djannati-Ataí 2003) collaborations and triggered a multiwavelength campaign involving radio, optical and X-ray observations (Krawczynski et al. 2004). The details of the very high energy (in this case for $E \geq 316\,\mathrm{GeV}$, and hereafter referred to as VHE) spectral analysis of the Whipple observations are presented here. Due to concerns over an observed reduction in the telescope efficiency for background cosmic ray events we have made an in-depth study of the systematics involved in the spectral analysis, the details of which are given in the following section.

2. The Whipple telescope and Data Analysis

The Whipple 10 m Imaging Atmospheric Cherenkov Telescope (IACT) is located at an altitude of 2.3 km on Mount Hopkins in Southern Arizona ($31^\circ\,40'\,30.8''$ latitude, $110^\circ\,57'\,6''$ longitude). A detailed description of the telescope can be found in Finley et al. (2001) and references therein, but briefly the telescope consists of a 10 m segmented mirror reflector of Davies-Cotton design and a 490 pixel photo-multiplier tube (PMT) camera. In this analysis only the high resolution (0.12° spacing) inner camera of 379 pixels has been used, covering a total field-of-view of 2.4°, in order to ensure a uniform response in the camera. The resultant images of the Cherenkov light from the air showers are parameterized according to Hillas (1985) and gamma-ray like images are selected using the "supercuts" criteria (Reynolds et al. 1993). The spectral analysis technique used in this study follows that detailed in Mohanty et al. (1998), for which we simulate the response of the detector to gamma-ray showers in order to allow an estimate of the energy of the primary gamma-ray for each individual event. The energy estimates are binned and convolved with a calculation of the effective collection area to obtain flux values as a function of energy. The spectrum is then compared to a hypothesised spectral form by means of a χ^2 minimisation. The gamma-ray selection cuts made in this spectral analysis are less strict than those in a standard supercuts analysis in order that a larger sample of gamma-rays (typically of order $\sim 90\%$) be kept in the resultant data-set and so making the effective collection area for the telescope less dependent on energy. The KASCADE code (Kertzman & Sembroski 1994) employing the GrISU version of detector code[1] was used to generate the simulated air showers for calculating the cut values and coefficients in the energy estimator function.

The data for the 1ES 1959 observations were taken in either of two observation modes and the analysis for these observation has been split according to the mode it was taken in, in order that the technicalities peculiar to the particular observation mode can be dealt with separately. In pair mode an off-source run (displaced by 30 minutes in right ascension) is taken contiguously with on-source data. This enables a measurement of the background cosmic-ray sample to be taken under as close an approximation to the atmospheric conditions present for the on-source data as possible. In tracking mode only the on-source observation is taken and the significance of the gamma-ray excess is calculated through the use of a tracking ratio; the ratio is found by utilising the large number of off-source runs that are taken during the same observing season as the tracking runs. The calculation of the tracking ratio is discussed in more detail in Horan et al. (2002). This mode of observation has the benefit of maximising the amount of time spent on a source, which is particularly useful

[1]obtainable at http://www.physics.utah.edu/gammaray/GrISU

when looking at short timescale flaring activity. The downside to the tracking method is that particular care needs to be taken in finding matching off-source runs in order to be able to do a spectral analysis (Petry et al. 2002).

2.1. Systematic errors in the spectral analysis

Reconstructing the energy spectrum of an observed gamma-ray flux requires an in-depth understanding of the detector properties and the stability of the detector with time. There are many potential reasons that detector response can change with time: ageing of the photo-multiplier tubes, degradation of mirror reflectivity and modifications to the telescope will all affect performance in ways that can introduce systematic errors into an analysis if not taken into account. In addition, the technique of ground-based gamma-ray astronomy relies on the atmosphere itself to provide the large collection area that makes it a viable technique. This means that it is very difficult to get a measure of every independent part of the detector chain and so several techniques are necessary to unfold the performance at different stages in order to determine the effective gain of the system.

Figure 1 shows the change in relative performance of the telescope as measured by two different methods: via the throughput (Le Bohec & Holder 2003) and through the imaging of muon rings (Rose et al. 1995; Rovero et al. 1996). These methods sample the atmosphere at different inputs into the chain and allow us to build up a picture of telescope's response to the light incident upon it and where changes are occurring. The throughput factor, which measures the telescope response to Cherenkov light produced by cosmic ray air showers, samples the most complete cross-section of the detector chain, incorporating the many kilometres of atmosphere associated with both shower generation and the attenuation of the resulting Cherenkov light generated by the shower particles. The muon ring images are sampling the local atmosphere (from $\sim$ 500 m above the telescope). The Cherenkov light output from a single muon is reasonably well understood and so acts in the place of a calibrated light source for the telescope. The common components to both methods are the reflection of the Cherenkov light at the mirrors and the conversion, amplification and digitisation of the light by the electronics chain. If the throughput of the telescope shows a decrease from run to run or season to season and the muon rings do not then we can be reasonably certain that some change in the atmosphere is affecting the performance of the detector; if both methods show a common change, be it an increase or decrease, as in figure 1, then we can be fairly certain it is due to a change in the telescope system itself.

There are additional subtleties that need to be taken into account when applying the throughput and muon-ring measurements to actual gamma-ray shower data. By far the

most numerous progenitors of extensive air showers are the hadronic cosmic-ray component which, having a larger mean free path, develop further into the atmosphere than their photon initiated counterparts. This means that the production and attenuation losses calculated for the throughput are only first order representative for gamma-ray showers; this can be compensated for by having accurate density and attenuation profiles for the atmosphere in the shower simulation code (Bernlohr 2000). Similarly, the muons being local to the telescope suffer much less severe attenuation losses and so provide a much bluer spectrum of Cherenkov light to the telescope system than the light from an air shower. This means that an accurate understanding of the optical properties of the telescope with wavelength, such as the mirror reflectivity and PMT quantum efficiency, is required. The fine points of the muon-ring analysis are less important in this study as we do not use the muon rings to provide an absolute gain calibration: instead we are looking for relative changes in performance in the muon data. The absolute calibration of the reflector and electronic gain for the simulations generated for this analysis is gauged through a series of detailed laboratory measurements.

Both the throughput and the muon ring measurements in figure 1 show a long term trend of performance loss. This demonstrates that it is due to something local at the telescope, i.e. not an atmospheric effect. Plotting the data points relative to their corresponding dark run in an earlier season, as opposed to just a single period, allows us to account for any seasonal variation in telescope performance. When plotted in such a way the points confirm the trend of a $\sim 12\%$ loss in gain seen in figure 1 and implies that a single factor is dominating the performance loss for the telescope. Tests applied to two PMTs from the camera in summer 2003 showed that the gains had dropped by $\sim 30\%$, which was compensated for by a systematic increase in the voltages applied to the PMTs at the start of the 2003-04 observing season.

The ability of the monitoring methods to accurately describe the changes of the detector system has been tested by evaluating the spectrum of the Crab Nebula from two datasets well separated in time. The Crab Nebula is the standard candle of VHE gamma-ray astronomy due to its stability and is therefore ideally suited to testing both deviations in telescope response and the methods for correcting those deviations. The spectrum for the Crab has been evaluated from observations taken in two periods either side of the 1ES 1959 observations. The exposure time for each dataset is of a similar size to that of the 1ES 1959 sample. The data for the Crab spectrum fit is from paired observations taken in February and December of 2002 (the details of the datasets are given in table 1). The telescope performance difference from its peak operating period was estimated from the change in throughput to be $\sim 12\%$ for the February data-set and $\sim 24\%$ for the December data-set. This correction was applied to the gain in the detector simulation code. The spectra can be seen in figure 2, they agree well with each other and with previously published values (Hillas et al. 1998).

The February and December Crab spectra can then be used to estimate the systematic errors in the analysis. By subjecting the earlier data-set to the correction applied to the later data-set and vice versa, the impact of the time varying component of the change in detector gain can be estimated. Then by varying where the correction is applied within the detector code – which could be applied to a reduced reflectivity component, mimicking a loss of Cherenkov photons, or a reduction in the electronics gain component, mimicking a fall in the photo-electron to digital count ratio, with nearly equal effectiveness. Both a reduced reflectivity and a reduced electronics gain would systematically lead to an underestimate of the primary photon's energy if not accounted for. For a power-law spectrum of the form

$$\frac{\mathrm{d}N}{\mathrm{d}E} = FE^{-\alpha}$$

where F is the flux constant and α the spectral index, then the additional uncertainty from this component to the flux constant $\delta F \simeq 6\%$ and to the spectral index $\delta\alpha \simeq 2.4\%$ per year of efficiency loss. These values are smaller than the statistical uncertainties for the following data, but not negligibly so, and are of a similar order to other systematic uncertainties that are common to a spectral analysis of VHE data.

3. Results of the 1ES 1959 spectral analysis

To take account of the effective collection area changing with the zenith angle of observation (θ_z), events were simulated in three zenith angle bins corresponding to the mid-point of a bin of width 0.1 in $1/\cos(\theta_z)$. This gives three simulation datasets centred at zenith angles of 36.9°, 42.2° and 46.4° respectively. The observational data are then split according to the relevant zenith angle bin and the spectrum calculated with the corresponding simulation dataset. The energy value of the first bin in a spectral fit is dependent on the zenith angle since the threshold energy of the telescope goes up with increasing zenith angle. For these observations and given the additional systematic uncertainties associated with the analysis the lowest reliable energy bin is centred at 383 GeV, as compared with 260 GeV under more ideal conditions (Krennrich et al. 2001). Spectra are calculated for each of the zenith angle data-sets and the data-points are then combined to calculate an average spectrum. To do this we took the average of the three flux constants calculated for the zenith angle subsets ($\overline{F} = 1/3(F_{36.9} + F_{42.2} + F_{46.4})$); the ratio of a data subset's flux constant to that average then acts as a weighting factor to all of the flux points in that subset's spectrum. Once all of the subsets have been weighted the χ^2 minimised best fit for the functional spectral form is found for all of the points. The deviation for this weighting process is added into the systematic uncertainty in the average flux constant. Using the centre of gravity of the points in this way helps avoid any one single point biasing the result disproportionately, but

it does mean the method will smooth out any change in spectral index with flux level, a matter dealt with in section 3.3.2.

All data, both simulated and actual telescope data, are subject to cleaning cuts of

- $0.4^\circ <$ distance $< 1.0^\circ$,
- the maximum signal in the 1^{st} highest tube > 50 digital counts,
- the maximum signal in the 2^{nd} highest tube > 45 digital counts,
- the maximum signal in the 3^{rd} highest tube > 40 digital counts.

to ensure that the Cherenkov light pool is being sampled in a region of linear density and that an event is well above the threshold of the detector electronics, which is a difficult region to simulate and could lead to unaccounted systematic uncertainties. A photo-electron is equivalent to about 3 digital counts.

In the following discussion, the quality of an on/off pair is a measure of how evenly matched the population of background cosmic-ray events between an on-source and an off-source run is. This number is determined in a region of parameter space where no gamma-ray signal should bias the result, which should be the case for events where the pointing angle $\alpha > 30^\circ$ (Hillas 1985; Reynolds et al. 1993). The significance of any excess events between the on- and off- data-sets is then calculated via the standard method as detailed in Li & Ma (1983). Since the cosmic-ray events should be isotropic on the sky there should be no appreciable difference between the number of cosmic-ray events between the on- and off-source observations: an excess significant at the $\geq 2.5\,\sigma$ level can be seen as there being a systematic difference in conditions between an on- and off- source run and that pair is then rejected for analysis.

3.1. May 2002 flare data

The May 2002 data for this dark run were taken in pair mode. The relevant parameters for the runs are given in table 2 along with the start time of the on-source run (in MJD; each run lasts for 28 minutes); the significance of the gamma-ray signal is calculated from super-cuts; the quality of the pair shows how well matched the background cosmic-ray populations for the on- and off-runs are prior to the spectral analysis.

The spectral fits to the data are shown in figure 3 and are given in table 3. Assuming

a pure power-law a spectrum of the form

$$\frac{\mathrm{d}N}{\mathrm{d}E} = (1.23 \pm 0.26_{\mathrm{stat.}} \pm 0.33_{\mathrm{sys.}}) \times 10^{-6} E^{-2.78 \pm 0.12_{\mathrm{stat.}} \pm 0.21_{\mathrm{sys.}}} \,\mathrm{m}^{-2}\,\mathrm{s}^{-1}\,\mathrm{TeV}^{-1},$$

is obtained with a $\chi^2 = 26.09$ for 19 degrees of freedom (d.o.f.). This spectral form is already an acceptable fit to the data and so looking for a more complex form at this time is not really warranted. A discussion on possible cut-offs to the spectrum is given later on.

3.2. 4th June 2002 flare

For the observations taken on the 4th June 2002, in order to maintain the maximum amount of on-source time, 1ES 1959 was observed in a tracking mode and therefore no equivalent off-source runs were taken for that particular night. As the flare for that night is of particular interest, due to the lack of an equivalent X-ray flare in RXTE data that was also being taken at that time as part of a multiwavelength campaign (Krawczynski et al. 2004), a special effort has been made to reconstruct the spectrum. Off-source runs have been selected to match the tracking observations based on a series of strict criteria such that they

- are within 5° in zenith angle to their corresponding tracking run;
- have pedestal fluctuations less than or equal to the track run, so that additional noise components are not added into the analysis;
- have a throughput within 0.05 of the track run in order that the runs are taken under similar atmospheric conditions;
- are within 1 month of the track observation in order that systematic changes in the telescope's effective gain are minimised;
- and are of good quality, i.e. within $2.5\,\sigma$ in the off-region ($\alpha > 30°$) after simple pre-spectral analysis cleaning cuts have been applied.

The last of these requirements ensures that the chosen off-source run accurately represents the cosmic-ray sample in the on-source run.

The details for this night's observations are given in table 4. The significance is calculated using an estimation of the cosmic-ray rate from the alpha distribution in the region $30° \leq \alpha \leq 60°$ called the tracking ratio (Horan et al. 2002), it is given as a reference to how

strong the flare was for that night's data. The spectral fit is then given in figure 4, for a pure power law the spectrum is best fit by

$$\frac{\mathrm{d}N}{\mathrm{d}E} = (1.07 \pm 0.16_{\mathrm{stat.}} \pm 0.57_{\mathrm{sys.}}) \times 10^{-6} E^{-2.82 \pm 0.15_{\mathrm{stat.}} \pm 0.3_{\mathrm{sys.}}} \,\mathrm{m}^{-2}\,\mathrm{s}^{-1}\,\mathrm{TeV}^{-1},$$

with a $\chi^2 = 10.98$ for 6 d.o.f., showing that once again a pure power-law is an adequate description of the 1ES 1959 spectrum. The increase in systematic uncertainty is introduced by having to find matching off-source runs to use in the analysis.

3.3. Spectral variability

How the spectrum behaves as a function of time and with the emission level of the object can give an insight into the underlying processes that are driving the emission. Variability is a clear indication of changes occuring at the source and could help to disentagle an internal process from an external one, such as absorption of the VHE flux on the extragalactic background light (EBL) (Krennrich et al. 2002; Hauser & Dwek 2001; Costamante et al. 2004). The data were therefore arranged into subsets in an attempt to measure any evolution of the spectral index.

3.3.1. As a function of time?

The May data were split into two subsets to check for any temporal variation in the spectral index. The first subset consisted of the three pairs taken on the night of the 17th May and the second subset of the remaining three pairs, one of each taken on the nights of the 18th, 20th and 22nd of May. The subset data were fit for a pure power-law spectral form only and the results are given in table 5. The difference in the spectral index for the two datasets is within, but at the bounds of, the error in spectral index.

3.3.2. As a function of flux?

There is clear evidence that the spectral shape of Mrk 421 varies as a function of emission state (Krennrich et al. 2002), with a power-law hypothesis being rejected and the spectrum hardening with increasing flux and a curvature term being present that shows no significant dependence on flux. If 1ES 1959 were to demonstrate a similar behaviour this would be very interesting. The data-runs were sub-divided into 4 minute bins and the activity calculated for each of these divisions. Three data-sets were then constructed: one for which the gamma-ray

rate was above 4 gamma-ray like events per minute; one for when it was between 2 and 4 per minute; and one for when the rate was lower than 2 per minute. Due to the fewer numbers of events in some of the split data-sets the binwidth in the spectral analysis was set to 0.33 in $\log(E)$, which is twice the width of the energy resolution function. Table 6 gives the spectral fit parameters for the three data subsets, once again only a pure power-law form was used to fit the points. Within the uncertainties there is no evidence to support a hypothesis of the spectral form changing with flux level in the 1ES 1959 data. It is worth remembering, though, that this data-set is still statistically limited and it was not until a sustained period of high activity in Mrk 421 provided good statistics that the spectral variation with flux state could be seen; the first spectrum calculated for Mrk 421, based on a brief flare, was also indicative of a pure-power law spectral form alone and could not lend strong support to the hypothesis of spectral variability either (Zweerink et al. 1997). Further observations of 1ES 1959 in a high state are required to be able to give a conclusive statement.

4. Conclusions and Discussion

The spectra of flares observed from 1ES 1959+650 in 2002 with the Whipple 10 m telescope have been calculated. The flaring behaviour, which was seen in conjunction with an X-ray flare in the May data and in the absence of a high X-ray state for the June data, is well fit by a pure power-law with a spectral index of $\alpha \simeq 2.8$ in both cases and shows no compelling evidence of variation within the experimental uncertainties, either in time or with flux level.

The value for the power-law spectral index in this flaring state is in good agreement with the value calculated by the HEGRA collaboration of $\alpha = 2.83 \pm 0.14_{\mathrm{stat.}} \pm 0.08_{\mathrm{sys.}}$ for energies above 1.4 TeV during the same time period (Aharonian et al. 2003). Since examining VHE spectra for cut-offs is of interest for those studying the distribution of the EBL (or intrinsic features) they also fit their data points with a spectral form that included an exponential cut-off term, found to be $\simeq 4.2$ TeV. If the cut-off observed in the Mrk 421 and Mrk 501 spectra (Krennrich et al. 2001; Aharonian et al. 2001) at ∼4–5 TeV were due to the EBL then we would expect any cut-off to the 1ES 1959 spectrum to become apparant at an energy below that due to the increased redshift of the object. Introducing an exponential cut-off term to the Whipple 10 m data for the May 2002 flare results in a best-fit of

$$\frac{\mathrm{d}N}{\mathrm{d}E} = (1.37 \pm 0.24_{\mathrm{stat.}}) \times 10^{-6} \exp\left(-\frac{E}{(11.2^{+7.7}_{-6.6})_{\mathrm{stat.}}\,\mathrm{TeV}}\right) E^{-2.39\pm0.26_{\mathrm{stat.}}}\,\mathrm{m}^{-2}\,\mathrm{s}^{-1}\,\mathrm{TeV}^{-1},$$

at a $\chi^2 = 24.9$ for 18 d.o.f. The errors reflect the fact that the value for the cut-off is correlated to the spectral index. Whilst larger than the value derived by the HEGRA group

in their observations it is close to 1 standard deviation of the uncertainties. Fixing to the HEGRA cut-off value of 4.2 TeV, but allowing the flux constant and spectral index to freely vary results in a χ^2 fit of 45.3, which gives a much lower confidence for there being a cut-off at that energy in the 1ES 1959 spectrum. The Whipple 10 m and HEGRA spectra are shown plotted together in figure 5, along with their power-law and exponential cut-off best fits. The difference in fluxes is not too worrying since the HEGRA observations were taken after the main flare occurred on the 17th May and so 1ES 1959 is expected to have a lower flux constant in the HEGRA data. Given the amount of time spent on-source for these observations and assuming that the steep value for the slope of the spectrum is correct and erring on the optimistic side of the effective collection area for the telescope staying constant once it peaks, even then one would assume there to be only ~ 40 photons detected by the 10 m in the last three bins combined – making those individual bins very sensitive to fluctuations. Observations made with new generation of instruments like VERITAS, H.E.S.S., MAGIC and CANGAROO III coming online (Krennrich et al. 2004; Hinton 2004; Lorenz 2004; Kubo et al. 2004) should improve the statistical quality of the spectrum due to their increased energy resolution and flux sensitivity. It is also possible that a cut-off is present at energies lower than can be reliably determined in the present data, the new generation of instruments with their lower threshold energies should also be able to resolve this matter.

We acknowledge the technical assistance of E. Roache and E. Little. This research is supported by grants from the U. S. Department of Energy, the National Science Foundation, the Smithsonian Institution, N. S. E. R. C. in Canada, Science Foundation Ireland and P. P. A. R. C. in the U. K.

REFERENCES

Aharonian, F. A. et al. 2003, A&A, 406, L9

Aharonian, F. A. et al. 2001, ApJ, 546, 898

Atoyan, A. M. et al. 2002, A&A, 383, 864

Bernlohr, K. 2000, A.Ph., 12, 255

Costamante, L. et al. 2004, New A Rev., 48, 469

Dermer, C. D., Schlickeiser, R. & Mastichiadis, A. 1992, A&A, 256, L27

Djannati-Ataí, A. 2002, in ASP Conf. Ser. 290, Active Galactic Nuclei: from Central Engine to Host Galaxy, ed. S. Collin, F. Combes and I. Shlosman, 291

Finley, J. P. et al 2001, in Proc. of the 27th ICRC (Hamburg) 7, ed. M. Simon, E. Lorenz & M. Pohl, 2827

Hauser, M. G. & Dwek, E. 2001, ARA&A, 39, 249

Hillas, A. M. 1985, in NASA Conf. Pub. 2376 Proc. of the 19th ICRC (La Jolla), 3, 445

Hillas, A. M. et al., 1998, ApJ, 503, 744

Hinton, J. A. for the HESS Collaboration, 2004, New A Rev., 48, 331

Holder, J., et al., 2003, ApJ, 583, L9-L12.

Horan, D. et al., 2002, ApJ, 571, 753

Kertzman, M. P. & Sembroski, G. H. 1994, Nucl. Instrum. & Methods Phys. Res. A 343, 629

Krawczynski, H., et al 2004, ApJ, 601, 151

Krennrich, F. et al., 2004, New A Rev., 48, 345

Krennrich, F. et al., 2002, ApJ, 575, L9

Krennrich, F. et al., 2001, ApJ, 560, L45

Kubo, H. et al., 2004, New A Rev., 48, 323

LeBohec, S. & Holder, J. 2003, A.Ph., 19, 221

Li, T.-P. & Ma, Y.-Q, 1983, ApJ, 272, 317

Lorenz, E., 2004, New A Rev., 48, 339

Maraschi, L. Ghisellini, G. & Celotti, A., 1992, ApJ, 397, L5

Mohanty G., et al. 1998, A.Ph., 9, 15

Mücke, A., et al., 2003, A.Ph, 18, 593

Petry, D. et al. 2002, ApJ, 580, 104

Reynolds, P. T. et al. 1993, ApJ, 404, 206

Rose, H. J., et al. 1995, in Proc. of the 24th ICRC (Rome), 3, 464

Rovero, A. C. et al. 1996, A.Ph, 5, 27

Sikora, M., Begelman, M. C. & Rees, M., 1994, ApJ, 421, 153

Zweerink, J. et al., 1997, ApJ, 490, L141

This preprint was prepared with the AAS LaTeX macros v5.2.

Date	time on-source [minutes]	significance σ	spectral fit $[\mathrm{m}^{-2}\,\mathrm{s}^{-1}\,\mathrm{TeV}^{-1}]$
February 2002	224 minutes	13.3	$\mathrm{d}N/\mathrm{d}E = (4.6 \pm 0.4) \times 10^{-7} E^{-2.55 \pm 0.10}$
December 2002	112 minutes	9.1	$\mathrm{d}N/\mathrm{d}E = (3.3 \pm 0.8) \times 10^{-7} E^{-2.45 \pm 0.35}$

Table 1: The details of the Crab data-set used in the study of the systematic effects in the spectral analysis. The errors for the spectral fit are statistical only, see the discussion in the text for an estimate of the systematic error.

Date [MJD]	significance	quality
52411.33125	$6.1\,\sigma$	$1.1\,\sigma$
52411.375	$7.3\,\sigma$	$-0.4\,\sigma$
52411.41667	$6.9\,\sigma$	$1.4\,\sigma$
52412.34097	$3.8\,\sigma$	$-1.1\,\sigma$
52414.40069	$7.5\,\sigma$	$2.1\,\sigma$
52416.43958	$4.1\,\sigma$	$1.2\,\sigma$
overall	$14.6\,\sigma$	$1.8\,\sigma$

Table 2: The statistics for the May 1ES1959 data-set. The significance is calculated after the application of supercuts (Reynolds et al. 1993; Finley et al. 2001) and measures the strength of the gamma-ray signal. The quality is calculated after the application of a looser set of cuts prior to spectral analysis and is a measure of how well matched the cosmic-ray sample for the on/off pair is.

E [TeV]	Flux $[\mathrm{m}^{-2}\,\mathrm{s}^{-1}\,\mathrm{TeV}^{-1}]$	δFlux
0.383	2.75×10^{-5}	1.0×10^{-5}
0.562	3.58×10^{-6}	2.1×10^{-6}
0.759	2.05×10^{-6}	7.5×10^{-7}
0.826	1.63×10^{-6}	6.8×10^{-7}
1.00	9.53×10^{-7}	5.5×10^{-7}
1.21	8.07×10^{-7}	2.4×10^{-7}
1.58	3.45×10^{-7}	9.2×10^{-8}
1.78	2.47×10^{-7}	9.6×10^{-8}
2.09	2.32×10^{-7}	7.7×10^{-8}
2.61	3.23×10^{-8}	3.8×10^{-8}
3.31	7.18×10^{-8}	2.0×10^{-8}
3.83	2.36×10^{-8}	1.6×10^{-8}
4.37	5.49×10^{-8}	1.4×10^{-8}
5.62	1.83×10^{-8}	6.6×10^{-9}
6.92	5.75×10^{-9}	3.3×10^{-9}
8.26	4.34×10^{-9}	3.1×10^{-9}
9.12	9.26×10^{-9}	2.6×10^{-9}
12.1	1.25×10^{-9}	1.1×10^{-9}
14.5	1.60×10^{-10}	4.2×10^{-10}
17.8	3.79×10^{-10}	2.7×10^{-10}
19.1	2.23×10^{-10}	5.8×10^{-10}

Table 3: Calculated fluxes for the May 2002 dataset.

Date [MJD]	significance	quality
52429.79861	$8.20\,\sigma$	$-0.89\,\sigma$
52429.81736	$10.07\,\sigma$	$0.33\,\sigma$
52429.83681	$8.34\,\sigma$	$-1.23\,\sigma$
overall	$15.3\,\sigma$	-1.04 σ

Table 4: The statistics for the June 1ES1959 data-set. The significance is calculated after the application of supercuts (Reynolds et al. 1993; Finley et al. 2001) to the matched pairs. The quality is calculated after the application of a looser set of cuts prior to spectral analysis and evaluates how well matched the cosmic-ray sample for the chosen on/off pair is.

data-set	observation time [minutes]	spectrum $[\mathrm{m}^{-2}\,\mathrm{s}^{-1}\,\mathrm{TeV}^{-1}]$	χ^2[d.o.f.]
1	84 min.	$\mathrm{d}N/\mathrm{d}E = (6.8 \pm 1.6) \times 10^{-7} E^{-2.41\pm0.21}$	4.53 [5]
2	84 min.	$\mathrm{d}N/\mathrm{d}E = (5.9 \pm 1.4) \times 10^{-7} E^{-2.63\pm0.15}$	12.15 [7]

Table 5: Spectra calculated after the data were split by time. Errors are statistical only. The degrees of freedom for the χ^2 fit are given in the square brackets.

rate [min^{-1}]	observation time [minutes]	spectrum [$\mathrm{m}^{-2}\,\mathrm{s}^{-1}\,\mathrm{TeV}^{-1}$]	χ^2[d.o.f.]
$\mathrm{R} < 2$	64 min.	$\mathrm{d}N/\mathrm{d}E = (5.1 \pm 1.2) \times 10^{-7} E^{-2.63 \pm 0.17}$	1.78 [4]
$2 < \mathrm{R} < 4$	76 min.	$\mathrm{d}N/\mathrm{d}E = (8.5 \pm 1.3) \times 10^{-7} E^{-2.47 \pm 0.14}$	2.51 [3]
$\mathrm{R} > 4$	24 min.	$\mathrm{d}N/\mathrm{d}E = (1.7 \pm 0.4) \times 10^{-6} E^{-2.78 \pm 0.13}$	6.69 [5]

Table 6: Spectra calculated after splitting the data according to flux level. Errors are statistical only. The degrees of freedom for the χ^2 fit are given in the square brackets.

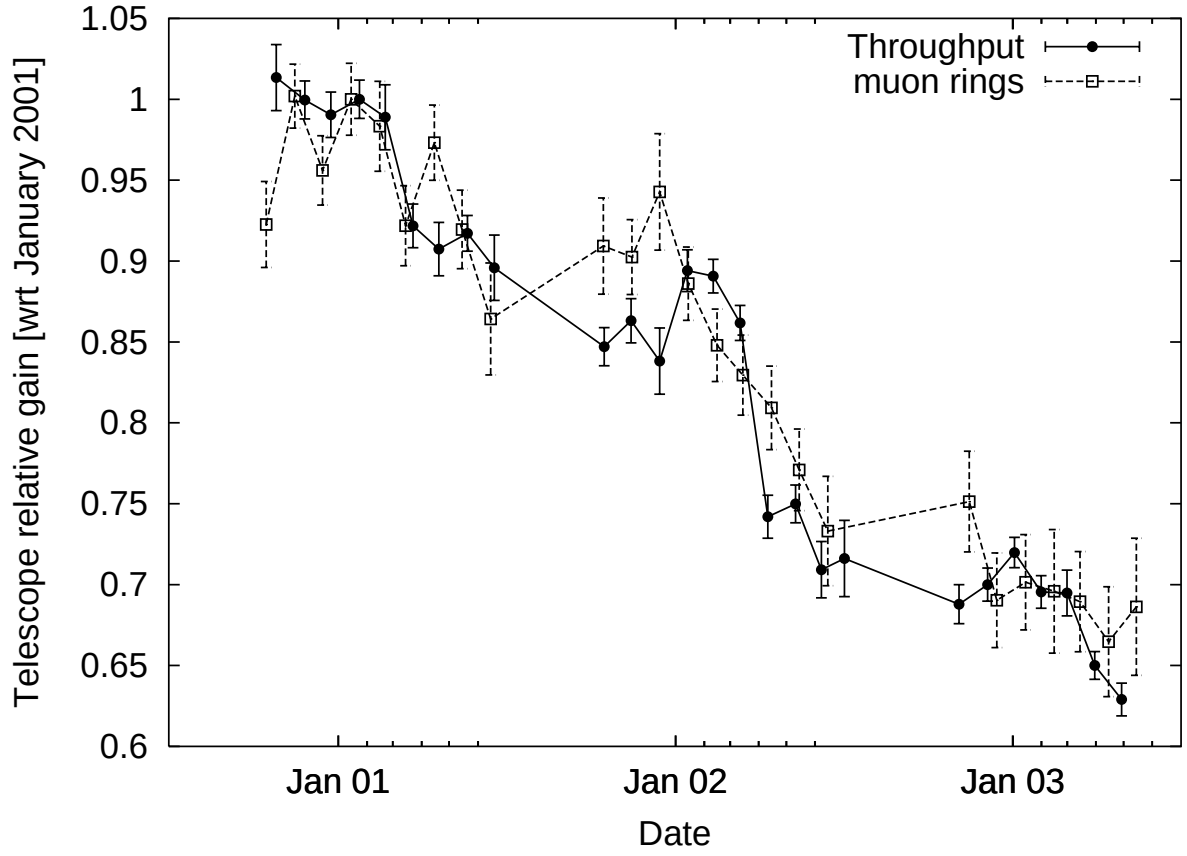

Fig. 1.— Charting the relative gain of the Whipple 10 m IACT over 3 observing seasons. The throughput samples the whole of the detector chain, whilst the muon rings tests the electronic, mechanical and local atmosphere (≤ 500 m above the telescope) only. The trend for both methods to show a loss in efficiency is indicative that it is not a change in atmospheric conditions that led to a decline in telescope performance.

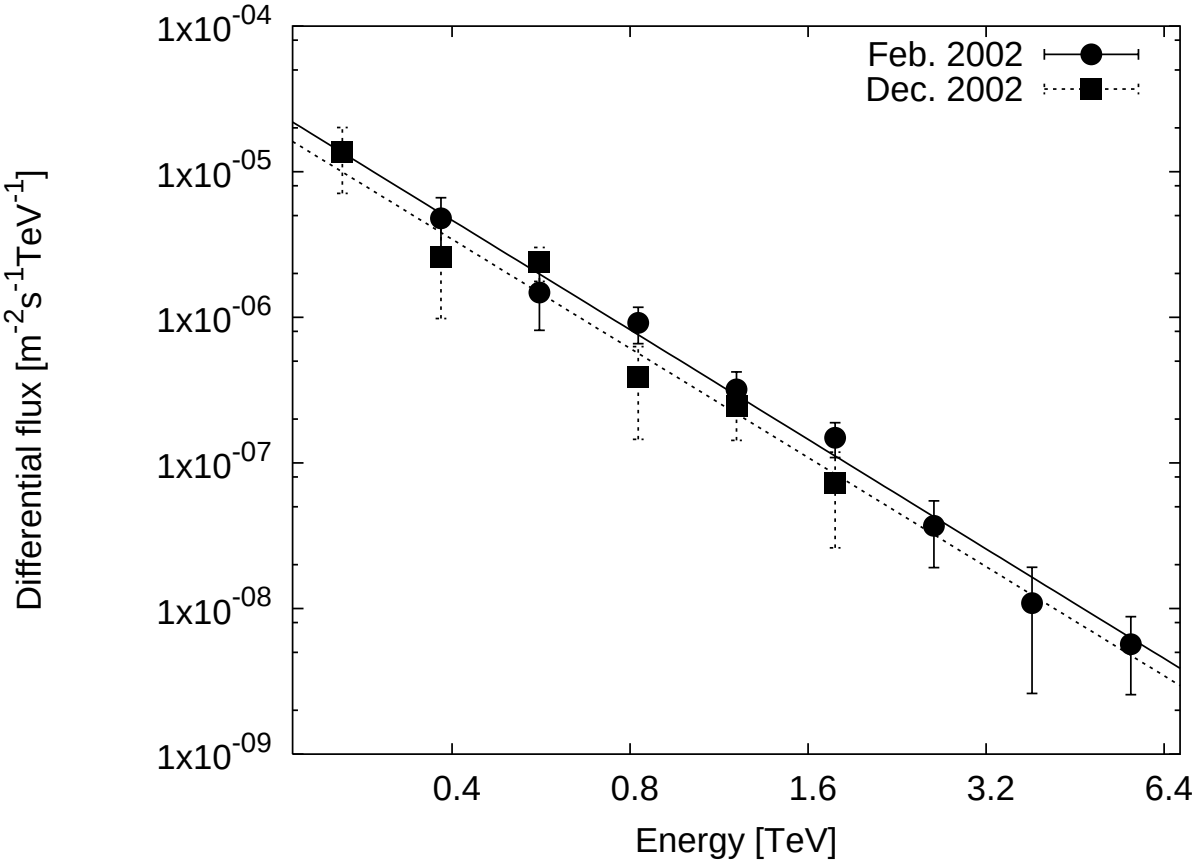

Fig. 2.— The spectra calculated for Crab Nebula data in 2002 during February (solid line) and December (dashed line).

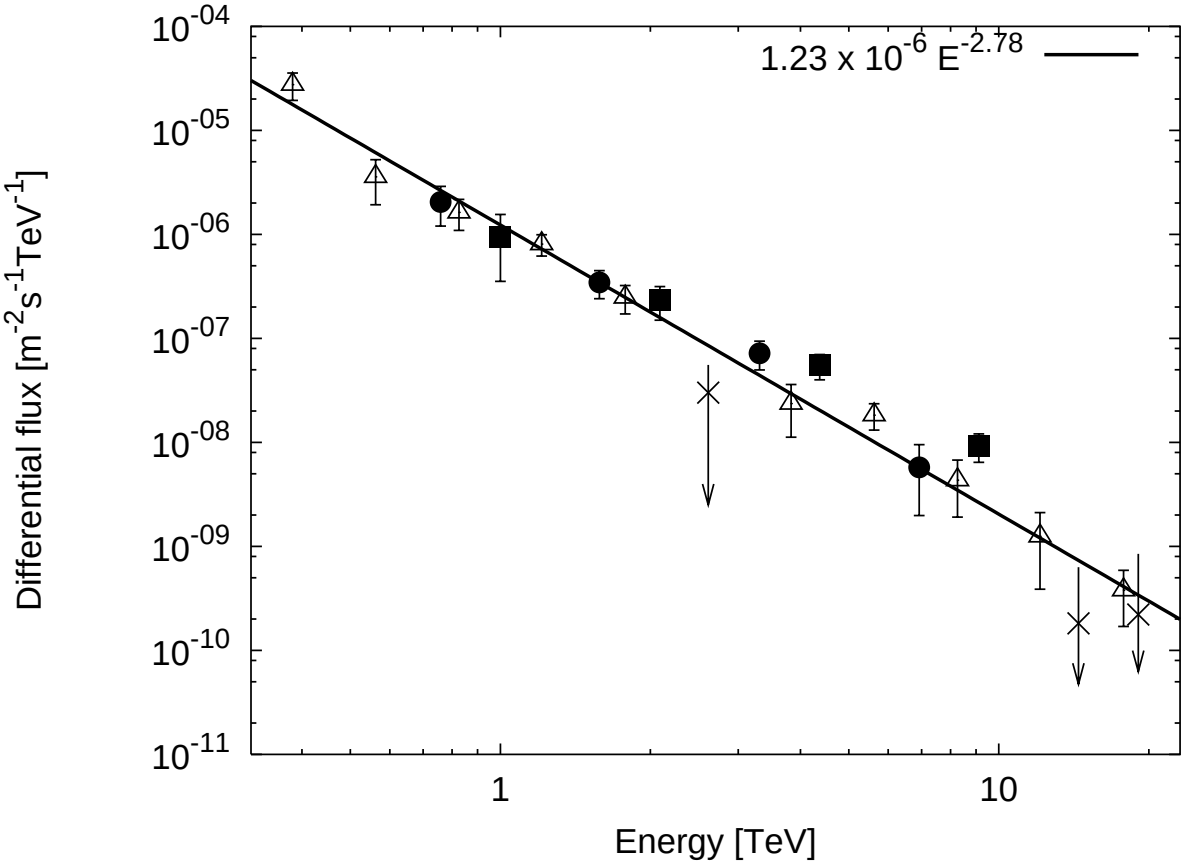

Fig. 3.— Spectrum calculated for the full May data-set after normalisation, the triangles mark the data-points for the 36.9° sub-set, the circles for the 42.2° sub-set and the squares the 46.4° sub-set. Crosses are for points where the uncertainty exceeds the calculated flux level. All points are included in the fit. The line is the best fit for a power-law spectrum to the normalised points.

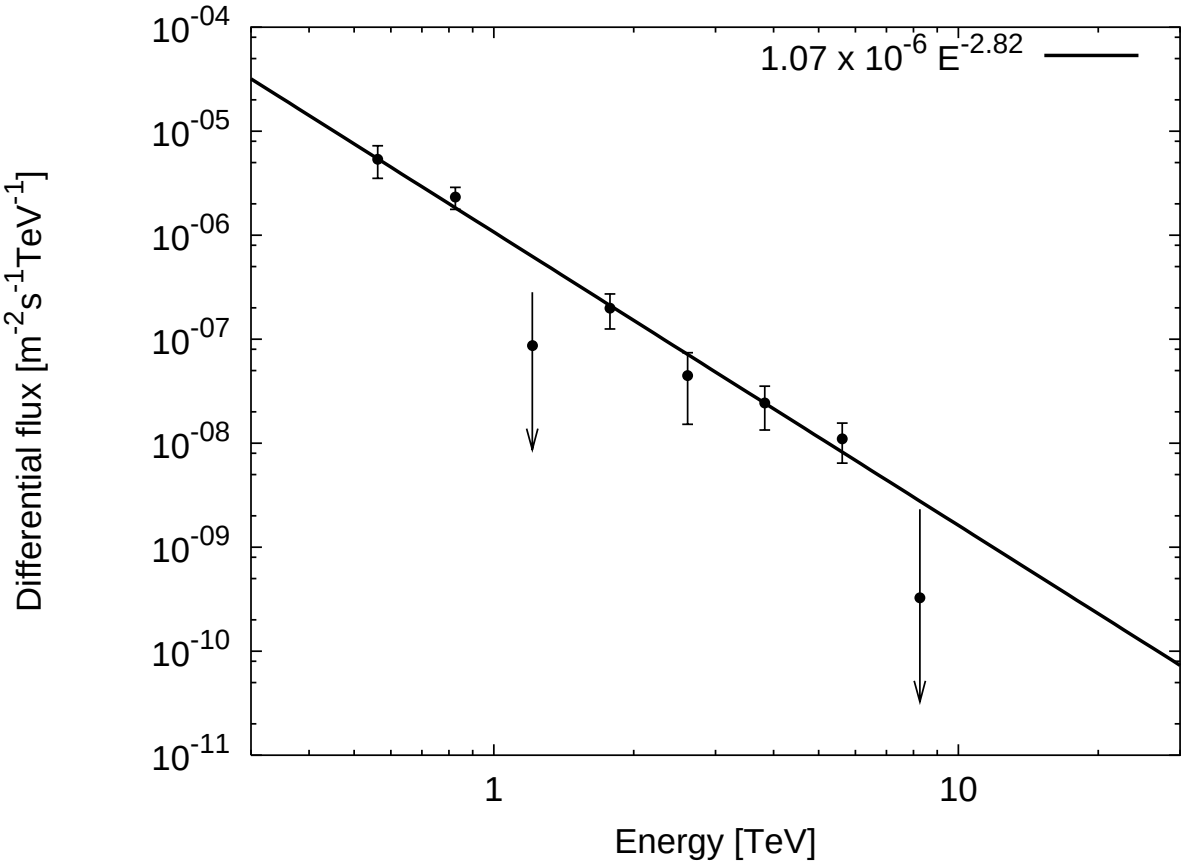

Fig. 4.— The spectrum as calculated for the flare on the 4th June.

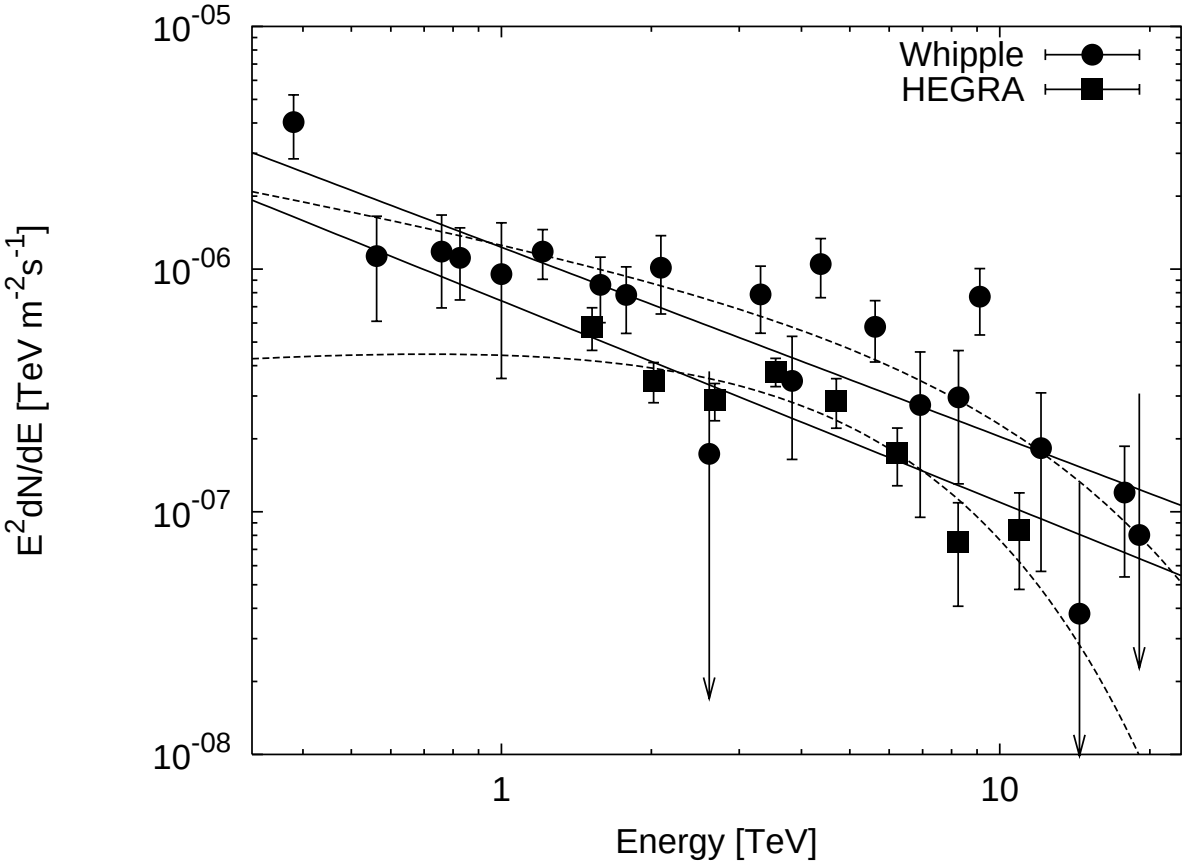

Fig. 5.— The May 2002 flare data, as in figure 3, but plotted as $E^2\mathrm{d}N/\mathrm{d}E$ instead in order to accentuate any structure that could be hidden by a steeply falling spectrum. Also plotted (the squares) are the data from HEGRA observations made during the same period (Aharonian et al. 2003). The resulting power law fits are shown as solid lines and fits including an exponential cut-off term as dashed lines (see text for discussion).